

## Evaluation of modified peanut shell in the removal of Cr(VI) from aqueous solution

Qian Li<sup>a,b,c,d,\*</sup>, Qing Huang<sup>a,b,c,d</sup>, Yifan Ruan<sup>a</sup>

<sup>a</sup>Department of Chemistry & Life Science, Hubei University of Education, Wuhan 430205, China, Tel. +86-27-87943929; email: liqian@hue.edu.cn (Q. Li), Tel. +86-27-87943929; email: 1733468464@qq.com (Q. Huang), Tel. +86-27-87943929; email: 370636668@qq.com (Y. Ruan)

<sup>b</sup>Hubei Environmental Purification Material Science and Engineering Technology Research Center, Hubei University of Education, Wuhan 430205, China

<sup>c</sup>Hubei Key Laboratory of Purification and Application of Plant Anti-Cancer Active Ingredients, Hubei University of Education, Wuhan 430205, China

<sup>d</sup>Hubei Engineering Technology Center of Environmental Purification Materials, Hubei University of Education, Wuhan 430205, China

Received 1 April 2022; Accepted 12 August 2022

### ABSTRACT

The use of agricultural wastes as low-cost and effective adsorbents is a promising path toward pollution reduction. This study aimed to investigate the adsorption ability of Cr(VI) by citric acid modified peanut shell (CPS). The adsorption equilibrium, kinetics, and thermodynamics were evaluated. The pseudo-first-order and pseudo-second-order models can be used to describe the uptake of Cr(VI) by CPS. The isotherm adsorption behavior was fully fitted with the Langmuir and Freundlich isotherm models, and the maximum adsorption capacity presented by the Langmuir model was 15.63 mg·g<sup>-1</sup>. Thermodynamic studies showed that the adsorption of Cr(VI) on CPS was an endothermic process. Negative values of  $\Delta G^\circ$  (between -7.28 and -6.60 kJ·mol<sup>-1</sup>) demonstrated that the adsorption process occurred spontaneously at all temperatures evaluated. Fourier-transform infrared spectroscopy, X-ray diffraction, carboxyl group content, and zeta potential measurements were used to clarify the structure of the adsorbent before and after modification and to discuss the possible adsorption mechanism. The scale-up design operation has been studied to show the cost-effective nature. The current work indicates that peanut shell treated with citric acid can be employed as a low-cost and potential adsorbent for removing Cr(VI) from aqueous solutions.

*Keywords:* Modified peanut shell; Citric acid; Chromium; Adsorption

### 1. Introduction

Water containing Cr(VI) has increased dramatically as a result of rapid industrial growth in electroplating, dye, mining, and many other industries [1,2]. Longer accumulation of Cr(VI) in the body may cause serious damages to skin, liver, kidney and nervous system. The maximum

acceptable limit of Cr(VI) in drinking water is about 0.05 mg·L<sup>-1</sup> according to the World Health Organization (WHO). Due to substantial environmental and health consequences, this type of industrial effluent must be treated before being released into the environment. However, Cr(VI) wastewater treatment is difficult because it is likely to interact with oxygen and exists as chromate and

\* Corresponding author.

dichromate, both of which are highly water-soluble and mobile in the environment [3,4].

Among various technologies such as chemical precipitation, reverse osmosis, electrochemical process, ion exchange, adsorption is considered to be one of the most preferred alternatives to remove Cr(VI) from industrial wastewater because of its convenience, reversibility, and low secondary pollution [5–7]. An essential factor of successful adsorptive applications is the adsorbent. Agricultural crops such as peanuts produce large quantities of shells that have little or no value, which are mostly served as animal feed or burned for energy, especially in China, which is the world's leading producer of peanuts, with an annual production capacity of 5 million tons of peanut shells. Based on their sustainability and biodegradability, converting these by-products into effective and low-cost bioadsorbents for heavy metal removal has attracted increasing research interest. Several studies have found that lignocellulosic materials such as peanut shell have high potential as bioadsorbents due to the fact that they are made up of D-glucose units containing free hydroxyl groups and carboxyl groups that can act as coordination sites to bind with various metal ions [8–11].

However, because of the low adsorption capacity, raw biosorbents are seldom directly applied for adsorption. To increase the number of functional groups or surface area and thereby improve adsorption performance, seeking green and sustainable ways to modify natural adsorbents is still a hot issue of research. It has been reported that citric acid (CA) can be used as a modifying agent to increase adsorption efficiency by introducing carboxylic functions to the structure of crude lignocellulosic materials, such as peach stone shell, sugarcane bagasse, cigarette fiber, almond, and hazelnut shell, through esterification reaction for wastewater treatment [12–15]. Therefore, the current study looked into the potential use of citric acid modified peanut shell (CPS) as an adsorbent for Cr(VI) removal, as well as the effect of CA on enhancing the ability of peanut shell to bind metal ions. The effects on adsorption capacity and removal efficiency, including adsorbent dose, initial concentration, contact time, and temperature, were investigated in detail. Adsorption kinetics, isotherms, and thermodynamic parameters were determined. In addition, X-ray diffraction (XRD), Fourier-transform infrared spectroscopy (FTIR), and  $\text{pH}_{\text{PZC}}$  were performed to characterize the synthesized adsorbents and to explore the adsorption mechanism. The scale-up design operation has been done as well to indicate the cost-effective nature of this study.

## 2. Materials and methods

### 2.1. Preparation of peanut shell powder modified with citric acid

The peanut shell (PS) used in the experiments was collected from a local market (Wuhan, China). The dried powders were pulverized and sieved to 80 mesh. After that, the peanut shell powder was mixed with 10% citric acid at a ratio of 1:40 (powder/acid, w/v) at 298 K for 3 h [16]. The obtained samples were then filtered, washed, dried and labeled as CPS. Analytical grade reagents were used in all cases.

### 2.2. Characterization

The raw PS and CPS were characterized by measuring the content of carboxyl group [17], the  $\text{pH}$  of point of zero ( $\text{pH}_{\text{PZC}}$ ), X-ray diffraction (XRD), and FTIR.

### 2.3. Adsorption of Cr(VI) on CPS

The adsorption capacity of Cr(VI) on CPS was studied by adding 2 g CPS into a series of 250 mL Cr(VI) solutions with different initial concentrations (5–70  $\text{mg}\cdot\text{L}^{-1}$ ) at 298 K for 6 h. The initial  $\text{pH}$  was adjusted to 2 by adding 1 M HCl. The residue Cr(VI) concentration was determined spectrophotometrically at 540 nm.

### 2.4. Calculation of adsorption capacity

The percentage (%) of removal can be calculated as:

$$\eta = \frac{C_0 - C_e}{C_0} \times 100\% \quad (1)$$

The adsorption capacity  $q_t$  ( $\text{mg}\cdot\text{g}^{-1}$ ) can be calculated as:

$$q_t = \frac{(C_0 - C_t)}{m} \times V \quad (2)$$

where  $\eta$  is the removal percentage,  $C_0$  ( $\text{mg}\cdot\text{L}^{-1}$ ) is the initial Cr(VI) concentration,  $C_t$  ( $\text{mg}\cdot\text{L}^{-1}$ ) is the residual Cr(VI) concentration at time  $t$  (min);  $V$  (L) is the volume of the solution, and  $m$  (g) is the dry weight of the adsorbent into each beaker.

### 2.5. Adsorption kinetics

Kinetics studies were carried out by preparing a series of 250 mL Cr(VI) solutions containing 2 g CPS with an initial concentration range of 5–70  $\text{mg}\cdot\text{L}^{-1}$  at different adsorption temperatures (298, 308, 323, 338, and 353 K). The  $\text{pH}$  was adjusted to 2 using 1 M HCl. Samples were collected at different time intervals and analyzed. Different kinetic models were applied to fit the adsorption process.

### 2.6. Pseudo-first-order kinetic model

The pseudo-first-order kinetic model can be given as follows [18]:

$$\log(q_e - q_t) = \log q_e - \frac{k_1 t}{2.303} \quad (3)$$

where  $q_e$  ( $\text{mg}\cdot\text{g}^{-1}$ ) and  $q_t$  ( $\text{mg}\cdot\text{g}^{-1}$ ) are amount of Cr(VI) adsorbed at equilibrium and at time  $t$  (min), respectively, and  $k_1$  ( $\text{min}^{-1}$ ) is the rate constant of pseudo-first-order adsorption.

### 2.7. Pseudo-second-order kinetic model

The pseudo-second-order kinetic model can be written as follows [19]:

$$\frac{t}{q_t} = \frac{1}{k_2 q_e^2} + \frac{t}{q_e} \quad (4)$$

where  $q_e$  ( $\text{mg}\cdot\text{g}^{-1}$ ) and  $q_t$  ( $\text{mg}\cdot\text{g}^{-1}$ ) are the amount of Cr(VI) adsorbed ( $\text{mg}\cdot\text{g}^{-1}$ ) at equilibrium and at time  $t$  (min), respectively, and  $k_2$  ( $\text{g}\cdot\text{mg}^{-1}\cdot\text{min}^{-1}$ ) is the rate constant of pseudo-second-order adsorption.

### 2.8. Elovich model

The linear form of Elovich equation can be generally expressed as follows [20]:

$$q_t = \frac{1}{\beta} \ln(\alpha\beta) + \frac{1}{\beta} \ln t \quad (5)$$

where  $\alpha$  ( $\text{mg}\cdot\text{g}^{-1}\cdot\text{min}^{-1}$ ) is the initial adsorption rate;  $\beta$  ( $\text{g}\cdot\text{mg}^{-1}$ ) is the desorption constant.

### 2.9. Weber and Morris intraparticle diffusion model

The Weber and Morris intraparticle diffusion model can be expressed as follows [21]:

$$q_t = k_{id} t^{1/2} + C \quad (6)$$

where  $q_t$  ( $\text{mg}\cdot\text{g}^{-1}$ ) is the amount of Cr(VI) adsorbed at time  $t$  (min),  $k_{id}$  ( $\text{mg}\cdot\text{g}^{-1}\cdot\text{min}^{1/2}$ ) is the rate constant of intraparticle diffusion, and  $C$  ( $\text{mg}\cdot\text{g}^{-1}$ ) is the intercept.

### 2.10. Boyd kinetic model

The Boyd kinetic model can be described as follows:

$$B_t = -0.4977 - \ln\left(1 - \frac{q_t}{q_e}\right) \quad (7)$$

$$B_t = k_b t + C \quad (8)$$

where  $B_t$  is Boyd constant,  $q_e$  ( $\text{mg}\cdot\text{g}^{-1}$ ) and  $q_t$  ( $\text{mg}\cdot\text{g}^{-1}$ ) are the amount of Cr(VI) adsorbed ( $\text{mg}\cdot\text{g}^{-1}$ ) at equilibrium and at time  $t$  (min), respectively.  $k_b$  and  $C$  are Boyd constants.

### 2.11. Adsorption isotherm

The isotherm studies were carried out by varying the initial Cr(VI) concentrations in the solution from 5 to 70  $\text{mg}\cdot\text{L}^{-1}$  at 298 K. The Langmuir, Freundlich, Temkin, and Dubinin–Radushkevich adsorption models were applied to characterize the adsorption mechanism.

### 2.12. Langmuir isotherm

The linear form of Langmuir isotherm can be expressed as [22]:

$$\frac{C_e}{q_e} = \frac{1}{bq_m} + \frac{C_e}{q_m} \quad (9)$$

where  $q_e$  ( $\text{mg}\cdot\text{g}^{-1}$ ) is the amount of Cr(VI) adsorbed at equilibrium,  $C_e$  ( $\text{mg}\cdot\text{L}^{-1}$ ) is the equilibrium concentration of Cr(VI),  $q_m$  ( $\text{mg}\cdot\text{g}^{-1}$ ) is maximum adsorption capacity,  $b$  ( $\text{L}\cdot\text{mg}^{-1}$ ) is the Langmuir constant.

$$\text{The separation factor } R_L = \frac{1}{1 + bC_0} \quad (10)$$

### 2.13. Freundlich isotherm

The linear form of Freundlich isotherm can be written as [23]:

$$\ln q_e = \frac{1}{n} \ln C_e + \ln K_f \quad (11)$$

where  $q_e$  ( $\text{mg}\cdot\text{g}^{-1}$ ) is the amount of Cr(VI) adsorbed at equilibrium,  $C_e$  ( $\text{mg}\cdot\text{L}^{-1}$ ) is the equilibrium concentration of Cr(VI),  $n$  is related to the intensity of adsorption,  $K_f$  ( $\text{mg}\cdot\text{g}^{-1}$ ) is the Freundlich constant.

### 2.14. Temkin–Pyzhev isotherm

The Temkin–Pyzhev isotherm can be shown as [24]:

$$q_e = \frac{RT \ln C_e}{b_T} + \frac{RT \ln A}{b_T} \quad (12)$$

where  $q_e$  ( $\text{mg}\cdot\text{g}^{-1}$ ) is the amount of Cr(VI) adsorbed at equilibrium,  $C_e$  ( $\text{mg}\cdot\text{L}^{-1}$ ) is the equilibrium concentration of Cr(VI),  $b_T$  ( $\text{J}\cdot\text{mol}^{-1}$ ) is the Temkin–Pyzhev isotherm constant related to the heat of adsorption,  $A$  ( $\text{L}\cdot\text{g}^{-1}$ ) is the Temkin–Pyzhev isotherm equilibrium binding constant corresponding to the maximum binding energy,  $R$  ( $8.314 \text{ J}\cdot\text{mol}^{-1}\cdot\text{K}^{-1}$ ) is the universal gas constant,  $T$  (K) is the absolute temperature.

### 2.15. Dubinin–Radushkevich isotherm

The Dubinin–Radushkevich isotherm can be described as [25]:

$$\ln q_e = -\beta \varepsilon^2 + \ln q_m \quad (13)$$

$$\varepsilon = RT \ln \left( 1 + \frac{1}{C_e} \right) \quad (14)$$

$$E = \frac{1}{(2\beta)^{1/2}} \quad (15)$$

where  $q_e$  ( $\text{mg}\cdot\text{g}^{-1}$ ) is the amount of Cr(VI) adsorbed at equilibrium,  $q_m$  ( $\text{mg}\cdot\text{g}^{-1}$ ) is maximum adsorption capacity,  $C_e$  ( $\text{mg}\cdot\text{L}^{-1}$ ) is the equilibrium concentration of Cr(VI),  $\varepsilon$  ( $\text{J}\cdot\text{mol}^{-1}$ ) is the Potential of Polanyi,  $\beta$  ( $\text{mol}^2\cdot\text{kJ}^{-2}$ ) is a constant related to the mean free energy of adsorption per mole of an adsorbate,  $R$  ( $8.314 \text{ J}\cdot\text{mol}^{-1}\cdot\text{K}^{-1}$ ) is the universal gas constant,  $T$  (K) is the absolute temperature, and  $E$  ( $\text{kJ}\cdot\text{mol}^{-1}$ ) is the mean adsorption energy.

### 2.16. Adsorption thermodynamics

$$\Delta G^\circ = \Delta H^\circ - T\Delta S^\circ \quad (16)$$

$$\Delta G^\circ = -RT \ln K_e = -RT \ln \frac{q_e}{C_e} \quad (17)$$

$$\ln \frac{q_e}{C_e} = -\frac{\Delta H^\circ}{RT} + \frac{\Delta S^\circ}{R} \quad (18)$$

where  $K_e$  is the distribution coefficient of the adsorbate, and  $q_e$  ( $\text{mg}\cdot\text{g}^{-1}$ ) is the amount of Cr(VI) adsorbed at equilibrium,  $C_e$  ( $\text{mg}\cdot\text{L}^{-1}$ ) is the equilibrium concentration of Cr(VI) in the solution.  $R$  ( $8.314 \text{ J}\cdot\text{mol}^{-1}\cdot\text{K}^{-1}$ ) is the universal gas constant and  $T$  (K) is the temperature.

### 3. Results and discussion

#### 3.1. Determination of carboxyl group content

Table 1 lists the values of the carboxyl group before and after modification. It was observed that CPS had a greater amount of carboxylic acid, indicating that the content of acid groups increased after reacting with citric acid, and the surface of CPS became more positive.

#### 3.2. Determination of $\text{pH}_{\text{PZC}}$

The point of zero charge ( $\text{pH}_{\text{PZC}}$ ) was used to determine the charge on the adsorbent surface. From Fig. 1 it was found that  $\text{pH}_{\text{PZC}}$  was 7.2 for PS and 6.6 for CPS. Accordingly, the adsorbent surface tended to be acidic due to the existence of acid groups in the peanut shell. This result was in agreement with that obtained for carboxyl group content. Because of the positive charge on the CPS surface, Cr(VI) adsorption was easier at pH values lower than 6.6.

#### 3.3. Effect of dosage on Cr(VI) adsorption

Fig. 2 depicts the effect of CPS dose on Cr(VI) adsorption capacity as contact time increases at an initial Cr(VI) concentration of  $10 \text{ mg}\cdot\text{L}^{-1}$ ,  $\text{pH} = 2$ ,  $298 \text{ K}$ . It was clear that as the dose increased, the adsorption capacity decreased from 2.34 to  $0.89 \text{ mg}\cdot\text{g}^{-1}$  after 4 h. And the adsorption

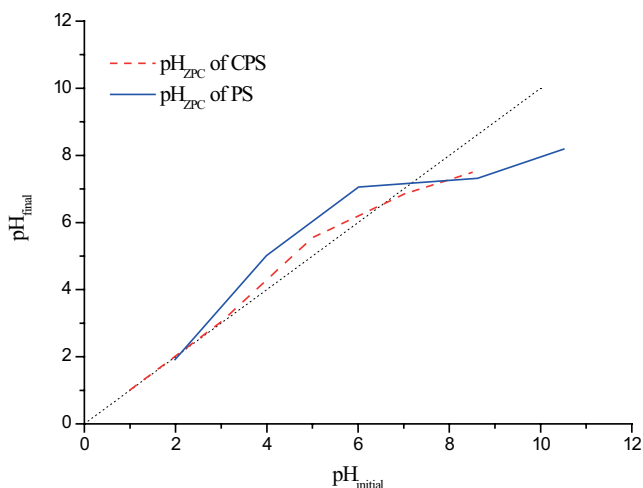


Fig. 1. Point of zero charge ( $\text{pH}_{\text{PZC}}$ ) of PS and CPS.

reached equilibrium within 240 min at doses of 2 and 3 g, which was much shorter than the equilibrium time at a dose of 1 g. However, when the dose was up to 3 g, the CPS could not be distributed evenly in solution, resulting in poor absorption. As a result, the optimum dose was determined to be 2 g for further experiments.

#### 3.4. Effect of initial concentration on Cr(VI) adsorption

Fig. 3 shows the effect of initial Cr(VI) concentration on Cr(VI) adsorption capacity as contact time increases at 2 g of CPS,  $\text{pH} = 2$ ,  $298 \text{ K}$ . Obviously, the adsorption process was rapid in the first 90 min and then gradually increased until the adsorption equilibrium plateau was reached. The fast adsorption of Cr(VI) at the initial stages may be due to the accessibility of the uncovered active sites on the surface of CPS and the strong driving force caused by the concentration gradient [14]. After 6 h, the Cr(VI) adsorption capacity increased from  $0.7$  to  $8.34 \text{ mg}\cdot\text{g}^{-1}$ , and the removal efficiency decreased from 99% to 92% within the initial Cr(VI) concentration range of  $5$  to  $70 \text{ mg}\cdot\text{L}^{-1}$ . As presented in Figs. 2 and 3, the contact time required for maximum adsorption of Cr(VI) by CPS was obviously dependent on the adsorbent dose and initial Cr(VI) concentration.

#### 3.5. Adsorption kinetics

In order to investigate the adsorption mechanism and identify the rate-limiting step, the adsorption data from Fig. 3 was analyzed through several kinetic models, such as pseudo-first-order, pseudo-second-order, Elovich, Weber–Morris, and Boyd kinetic models (Fig. 4). Tables 2 and 3 summarize the derived parameters from these corresponding plots.

Table 1  
Content of carboxyl groups of PS and CPS

| Adsorbent | Value ( $\text{mmol}\cdot\text{g}^{-1}$ ) |
|-----------|---|
| PS        | 3.28                                      |
| CPS       | 3.44                                      |

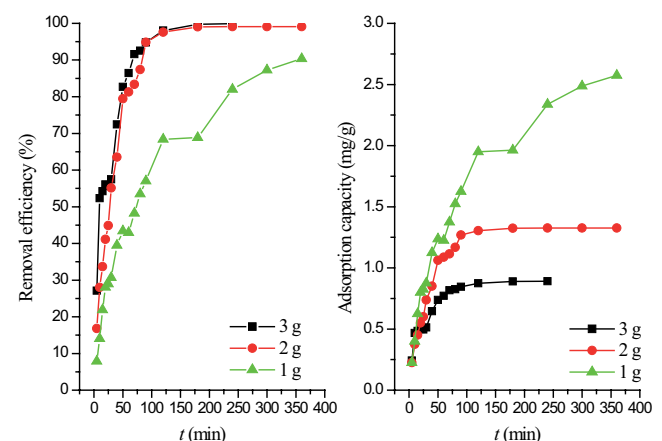


Fig. 2. Effect of adsorbent dosage on Cr(VI) adsorption.

For varying initial concentrations, the plots of  $\log(q_e - q_t)$  vs.  $t$  and  $t/q_t$  vs.  $t$  for the pseudo-first-order model and pseudo-second-order model both showed straight lines, as indicated in Fig. 4a and b. The rate constant  $k$  and

equilibrium adsorption capacity  $q_{e,cal}$  could be calculated from the slopes and intercepts of the corresponding linear plots.

As listed in Table 2, the relatively high value of  $R^2$  ( $>0.99$ ) suggested that both pseudo-first-order and pseudo-second-order kinetic models were suitable to describe this adsorption kinetic process at different Cr(VI) concentrations. However, a slight difference between  $q_{e,exp}$  and  $q_{e,cal}$  was found in the case of the pseudo-second-order kinetic model. The calculated values of  $q_{e,exp}$  (0.69, 0.95, 1.47, 2.66, and  $8.35 \text{ mg}\cdot\text{g}^{-1}$ ) from the pseudo-first-order kinetic model were much closer to the experimental values  $q_{e,exp}$ . Other researchers have also reported similar observations [26–28].

The Elovich equation is one of the most useful models for modeling adsorption involving chemisorption [29]. The fitting results of the Elovich model are given in Fig. 4c and Table 2. As the initial Cr(VI) concentration increased, the initial adsorption rate constants  $\alpha$ , increased from 0.06 to  $0.28 \text{ mg}\cdot\text{g}^{-1}\cdot\text{min}^{-1}$ , whereas the surface coverage constant,  $\beta$ , decreased from 4.78 to  $0.50 \text{ g}\cdot\text{mg}^{-1}$ . Therefore, increasing the Cr(VI) concentration might increase the rate of chemisorption but decrease the surface coverage of chromium ions. The linear regression correlation coefficients

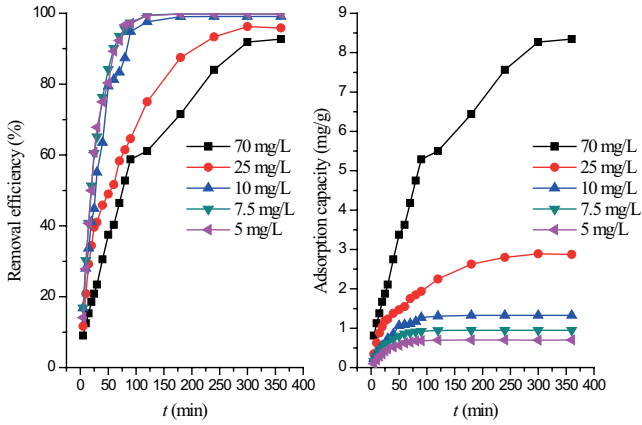


Fig. 3. Effect of initial concentration on Cr(VI) adsorption.

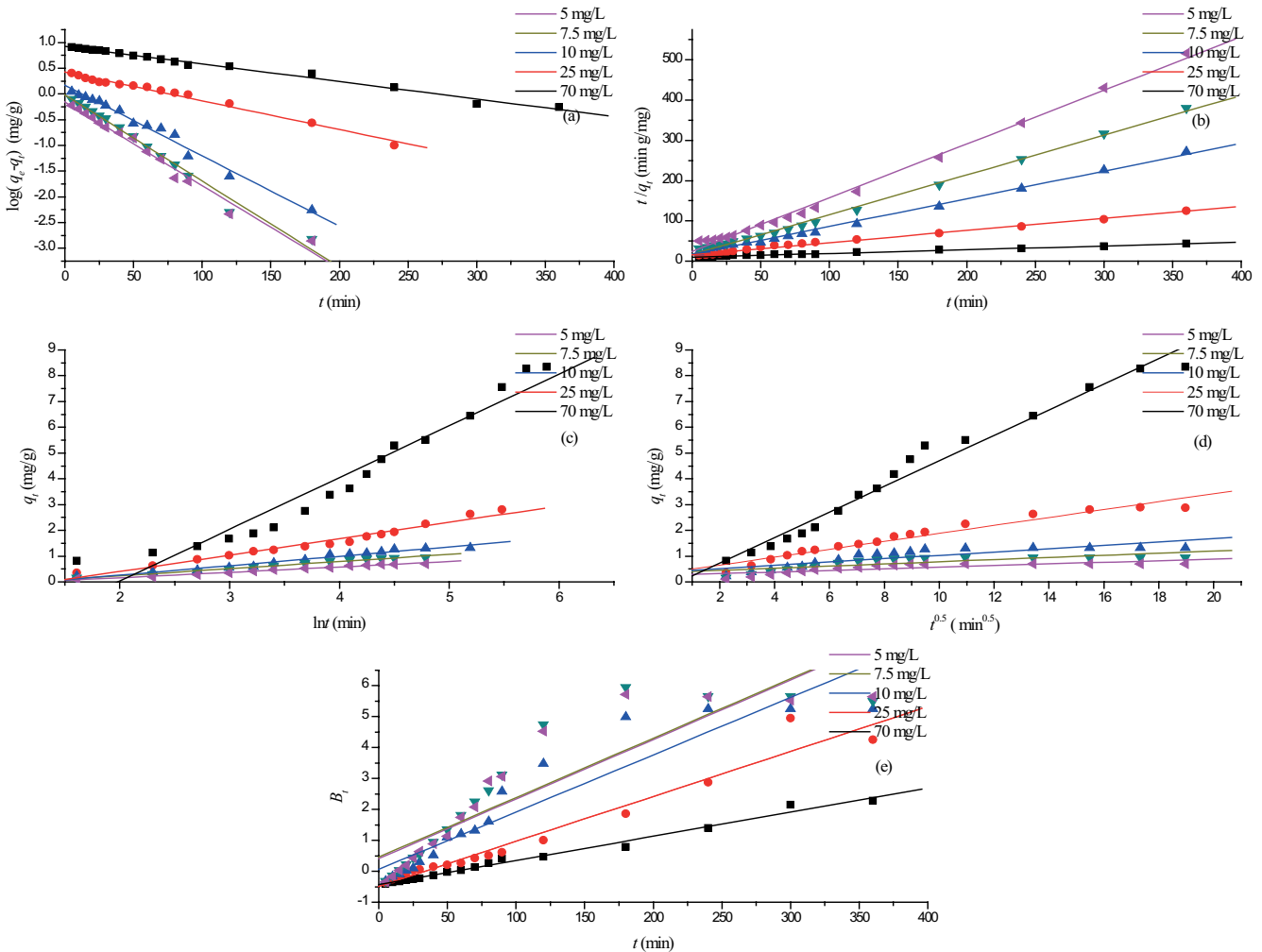


Fig. 4. Adsorption kinetics for Cr(VI) adsorption onto CPS: (a) pseudo-first-order kinetic model, (b) pseudo-second-order kinetic model, (c) Elovich kinetic model, (d) Weber–Morris intraparticle diffusion model, and (e) Boyd’s film diffusion model.

Table 2  
Pseudo-first-order, pseudo-second-order, and Elovich parameters for adsorption of Cr(VI) at different initial concentrations

| $C_0$<br>(mg·L <sup>-1</sup> ) | $q_{e,exp}$<br>(mg·g <sup>-1</sup> ) | Pseudo-first-order                    |                               |        | Pseudo-second-order                   |  |        | Elovich  |                                  |        |
|--------------------------------|--------------------------------------|---------------------------------------|-------------------------------|--------|---------------------------------------|--|--------|--|----------------------------------|--------|
|                                |                                      | $q_{1e,cal}$<br>(mg·g <sup>-1</sup> ) | $k_1$<br>(min <sup>-1</sup> ) | $R^2$  | $q_{2e,cal}$<br>(mg·g <sup>-1</sup> ) | $k_2$<br>(g <sup>-1</sup> ·mg <sup>-1</sup> ·min <sup>-1</sup> ) | $R^2$  | $\alpha$<br>(mg·g <sup>-1</sup> ·min <sup>-1</sup> ) | $\beta$<br>(g·mg <sup>-1</sup> ) | $R^2$  |
| 5                              | 0.7                                  | 0.69                                  | $3.73 \times 10^{-2}$         | 0.9903 | 0.75                                  | $7.32 \times 10^{-2}$  | 0.9977 | $6.10 \times 10^{-2}$                                | 4.78                             | 0.9931 |
| 7.5                            | 0.95                                 | 0.95                                  | $3.85 \times 10^{-2}$         | 0.9927 | 1.01                                  | $5.89 \times 10^{-2}$  | 0.9983 | 8.72   | 3.59                             | 0.9922 |
| 10                             | 1.33                                 | 1.47                                  | $3.15 \times 10^{-2}$         | 0.9924 | 1.45                                  | $2.74 \times 10^{-2}$  | 0.9977 | 0.1  | 2.74                             | 0.9800 |
| 25                             | 2.9                                  | 2.66                                  | $1.29 \times 10^{-2}$         | 0.9932 | 3.32                                  | $5.70 \times 10^{-3}$  | 0.9963 | 0.16   | 1.57                             | 0.9850 |
| 70                             | 8.9                                  | 8.35                                  | $7.83 \times 10^{-3}$         | 0.9942 | 10.79                                 | $8.88 \times 10^{-4}$  | 0.9896 | 0.28   | 0.5                              | 0.9688 |

Table 3  
Parameters of Weber–Morris intraparticle and Boyd’s film diffusion model for Cr(VI) adsorption at different initial concentrations (0–360 min)

| $C_0$<br>(mg·L <sup>-1</sup> ) | $k_{id}$<br>(mg·g <sup>-1</sup> ·min <sup>1/2</sup> ) | $C$<br>(mg·g <sup>-1</sup> ) | $R^2$  | $k_b$<br>(min <sup>-1</sup> ) | $C$<br>(mg·g <sup>-1</sup> ) | $R^2$  |
|--------------------------------|---|------------------------------|--------|-------------------------------|------------------------------|--------|
| 5                              | 0.0315  | 0.2566                       | 0.8054 | 0.0192                        | 0.4137                       | 0.9063 |
| 7.5                            | 0.0418  | 0.3617                       | 0.8045 | 0.0192                        | 0.4607                       | 0.8965 |
| 10                             | 0.0657  | 0.3737                       | 0.8598 | 0.0185                        | 0.0622                       | 0.9378 |
| 25                             | 0.1541  | 0.3418                       | 0.9754 | 0.0148                        | -0.4876                      | 0.9785 |
| 70                             | 0.4962  | -0.267                       | 0.9882 | 0.0078                        | -0.4342                      | 0.9942 |

at 5, 7.5, 10, 25 and 70 mg·L<sup>-1</sup> were 0.9931, 0.9922, 0.98, 0.985 and 0.9688, respectively, which were all inferior to those of pseudo-first-order and pseudo-second-order kinetic models, suggesting the insufficiency of Elovich model for explaining the relationship between Cr(VI) and CPS.

In order to further identify the diffusion mechanism, the Weber–Morris intraparticle diffusion and Boyd models were considered. The plot of  $q_t$  vs.  $t^{1/2}$  for the intraparticle diffusion model is shown in Fig. 4d, and the values of  $k_{id}$  and  $C$  are obtained from the slopes and intercepts of the plots, respectively (Table 3).

According to Table 3, internal diffusion was not the only rate-controlling step because none of the plots were completely linear or passed through the origin in the range studied. The deviation from the origin might be caused by the difference between the initial rate and final rate of mass transfer. Furthermore, the value of intercept  $C$  provides an impression of the thickness of the boundary layer. The surface sorption or the boundary layer effect might contribute more to the rate-determining step when the intercept  $C$  is larger. Accordingly, the interaction between Cr(VI) ions and CPS was either restricted to the surface or to the pores of the adsorbent.

The experimental data was further assessed by the Boyd model. Five fitting curves, as shown in Fig. 4e, had a linear trend, but none of them passed through the origin. Therefore, the process was governed by intraparticle and film diffusion simultaneously, which supported the outcomes of the intraparticle diffusion model. Nevertheless, the comparison indicated that both the Weber–Morris and Boyd models exhibited lower  $R^2$  values than those of the previous kinetic models, especially at lower initial Cr(VI) concentrations.

As a result, the adsorption kinetics followed the pseudo-first-order, pseudo-second-order, and Elovich models better than the Weber–Morris and Boyd kinetic models to predict the adsorption of Cr(VI) onto CPS in the experimental range. The adsorption behaviors were complex, involving multiple rate-controlling steps.

### 3.6. Adsorption isotherms

Several isotherm models (Langmuir, Freundlich, Temkin–Pyzhev, and Dubinin–Radushkevich) were used to fit the equilibrium data of Cr(VI) adsorption onto CPS. Based on the fitting results of isotherm models, an appropriate adsorption isotherm mechanism can be identified.

The Langmuir model implies that adsorbate molecules are adsorbed through monolayer adsorption at specific homogeneous sites with no interaction between adsorbed molecules. Table 4 shows the fitting parameters and correlation coefficients ( $R^2$ ) obtained from the linear regression analysis of the Langmuir isotherm at 298 K (Fig. 5a).

The maximum Cr(VI) adsorption capacity, as specified by the Langmuir model, was 15.63 mg·g<sup>-1</sup>, with an  $R^2$  of 0.9961. The high value of  $R^2$  showed the suitability of the Langmuir isotherm. In addition, the essential characteristics of the Langmuir isotherm can be expressed by a dimensionless separation factor,  $R_L$ . The  $R_L$  values calculated from Eq. (10) were in the range of 0.01–0.15 for the initial Cr(VI) concentration ranging from 5 to 70 mg·L<sup>-1</sup>. This parameter value ( $0 < R_L < 1$ ) indicated the favorable nature of the adsorption of Cr(VI) on CPS.

The Freundlich isotherm assumes that adsorption takes place on heterogeneous surfaces with a

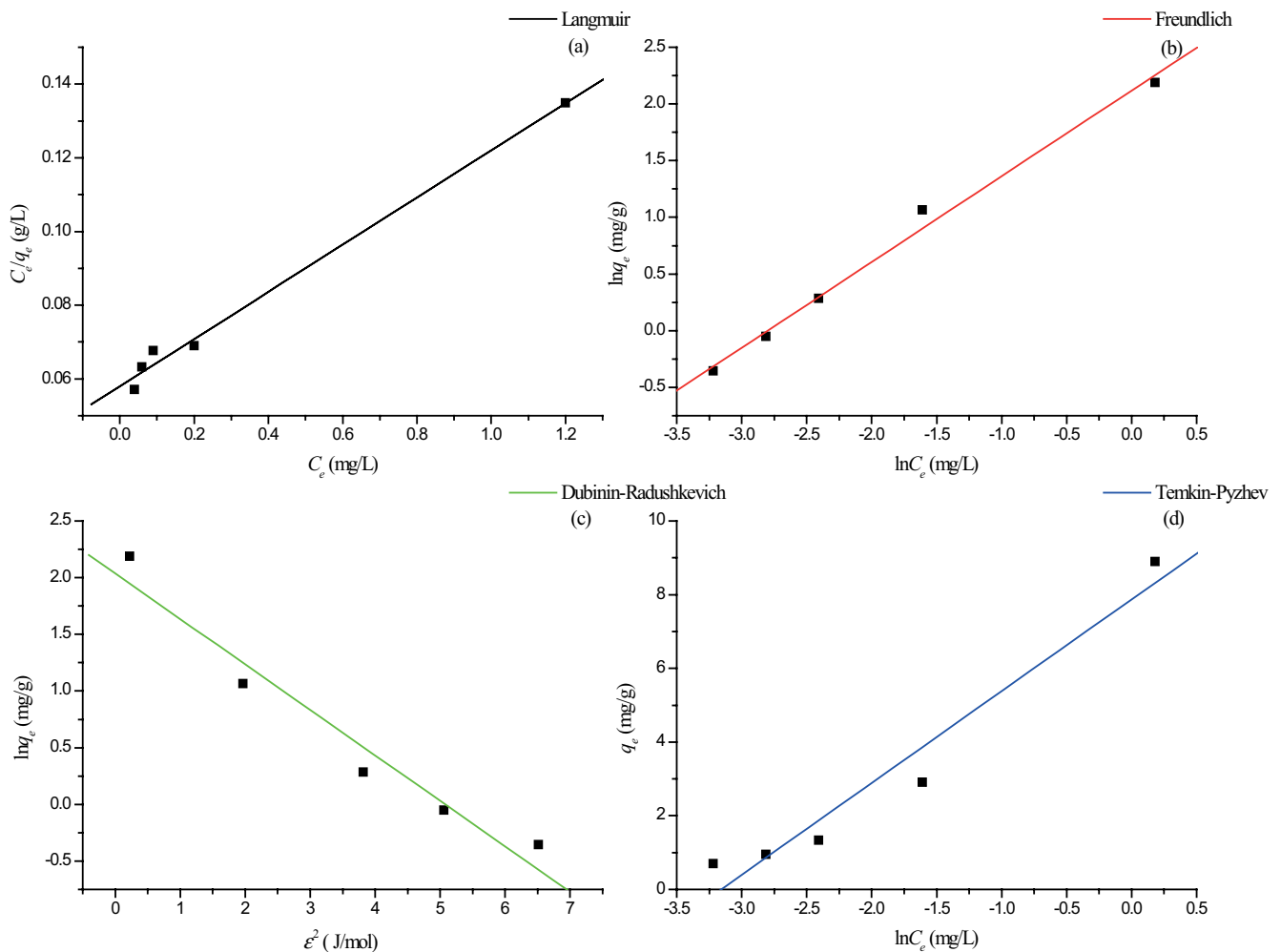


Fig. 5. Adsorption isotherms for Cr(VI) adsorption onto CPS at 298 K: (a) Langmuir adsorption isotherm, (b) Freundlich adsorption isotherm, (c) Dubinin–Radushkevich adsorption isotherm, and (d) Temkin–Pyzhev adsorption isotherm.

non-uniform distribution of adsorption heat. The heterogeneity arises from the existence of surface functional groups and adsorbent–adsorbate interactions [30]. According to the linear Freundlich isotherm plot (Fig. 5b), it was noted that the Freundlich isotherm also fitted the experimental data well, as a high  $R^2$  was observed (Table 4). The Freundlich isotherm constants  $K_F$  and  $n$  were  $8.31 \text{ mg}\cdot\text{g}^{-1}$  and 1.32, respectively. The value of  $n$  represented the favorable adsorption nature of Cr(VI) by CPS.

Consequently, the applicability of Langmuir and Freundlich isotherms suggested that the monolayer and heterogeneous coverage of the adsorbate be formed on the adsorbent surface and the adsorption of Cr(VI) on CPS was a complicated process including physical, chemical, monolayer, and multilayer adsorption. This result was consistent with other results published in the literature [31].

The Dubinin–Radushkevich isotherm model is typically employed to distinguish whether the adsorption is a physical or chemical process on the basis of a Gaussian energy distribution on the heterogeneous surface. If the mean adsorption free energy  $E$  is between 8 and  $16 \text{ kJ}\cdot\text{mol}^{-1}$ ,

the adsorption behavior can be described by chemical ion exchange; if  $E$  is less than  $8 \text{ kJ}\cdot\text{mol}^{-1}$ , the adsorption is controlled by a physical process [32]. The Dubinin–Radushkevich isotherm parameters and correlation coefficients are given in Fig. 5c and Table 4. It was found that the calculated value of  $E$  was  $1.12 \text{ kJ}\cdot\text{mol}^{-1}$  under the studied experimental conditions, indicating that there might be a physical adsorption mechanism involved in the process.

The Temkin isotherm assumes that the adsorption heat decreases linearly with coverage because of adsorbate–adsorbate interaction and those binding energies are distributed homogeneously [33]. Fig. 5d shows the linear fitting for the Temkin isotherm, and the values of the isotherm parameters are given in Table 4. As depicted in Table 4, the Temkin constants,  $b_T$  and  $A$ , were calculated to be  $997.97 \text{ J}\cdot\text{mol}^{-1}$  and  $23.58 \text{ L}\cdot\text{g}^{-1}$ , respectively. The  $R^2$  value of the Temkin model was relatively lower than other models but still greater than 0.97, implying that although the Temkin model was not the best of the four models studied so far, the electrostatic interaction might be included between Cr(VI) and CPS.

### 3.7. Adsorption thermodynamics

To evaluate the feasibility of this study, the thermodynamic parameters  $\Delta H^\circ$ ,  $\Delta S^\circ$  and  $\Delta G^\circ$  were obtained by using Eqs. (16)–(18) as shown in Table 5.

Table 5 showed that over the temperature range of 298–348 K, the values of  $\Delta H^\circ$  and  $\Delta G^\circ$  were found to be negative, indicating that the interaction between CPS and Cr(VI) was a favorable, feasible, spontaneous, and exothermic adsorption process. Similar findings were presented in the previous studies [34]. The negative value of  $\Delta S^\circ$  showed the adsorption caused the decrease in disorder at the interface between the adsorbent and the solution phase.

### 3.8. Possible adsorption mechanism

To further explore the mechanism of Cr(VI) adsorption on CPS, XRD and FTIR analysis were conducted.

Fig. 6 shows the XRD patterns of PS and CPS before and after adsorption. The native PS depicted obvious diffraction peaks at  $2\theta \approx 15^\circ$ ,  $17^\circ$ ,  $22^\circ$ , and  $35^\circ$  that corresponded to the characteristic peaks of natural cellulose types I and II [35]. Nevertheless, the XRD pattern of CPS showed a much broader peak distribution than that of PS. The degree of crystallinity of PS decreased after being treated with citric acid, which is due to the damage in the crystal structure caused by reacting with citric acid. The amorphous phase of both PS and CPS was confirmed by the presence of fewer peaks, which could indicate that chromium ions could penetrate and stay on the surface of the adsorbent. This observation was in agreement with the previous studies [36,37]. Nevertheless, the peaks at about  $15^\circ$  and  $17^\circ$  decreased after Cr(VI) adsorption compared to the XRD pattern before adsorption, indicating an interaction between CPS and chromium ions.

Fig. 7 shows the FTIR spectra of PS and CPS before and after adsorption. In the structure of pure peanut shell, the bands presented at 2,810; 1,391; and  $1,351\text{ cm}^{-1}$  indicated the aliphatic C–H group (Fig. 7a). These bands were weaker in the structure of CPS (Fig. 7b). The peak observed at approximately  $1,596\text{ cm}^{-1}$  represented the C–O stretch. This point has shifted to  $1,587\text{ cm}^{-1}$  in CPS. The peak shown at  $1,253\text{ cm}^{-1}$  verified the presence of –C–O peaks. The peaks in the range of  $1,025\text{--}1,097\text{ cm}^{-1}$  referred to the C–O–C structure. These points have been lost in the structure of CPS. Furthermore, the peak at about  $1,642\text{ cm}^{-1}$  was

noted as evidence that the carboxyl groups originated from citric acid. Accordingly, the esterification between citric acid and peanut shell occurred, and the peanut shell had the required functional groups to be a potential adsorbent for Cr(VI) uptake. In contrast, peak intensities of at 3,441; 1,645; 1,109; and  $762\text{ cm}^{-1}$  decreased after adsorption, while peaks at  $1,385\text{ cm}^{-1}$  showed a slight shift in transmittance (Fig. 7c), indicating that the –OH, –NH<sub>2</sub>, –C=C, C–N groups, and  $\pi\text{--}\pi$  interactions played a role in the Cr(VI) adsorption process [38]. This result coincided with those obtained by Altun et al. [15], Leng et al. [39], and Wang et al. [40].

Based on the analysis above, CPS provided characteristics including amorphous structure, acidic pH<sub>pZC'</sub> and functional groups of –OH, –NH<sub>2</sub>, and –C=O, which were favorable for the adsorption of Cr(VI). After citric acid treatment, the surface of the peanut shell was positively charged at an experimental pH (pH = 2). Since the dominant species of Cr(VI) at acidic pHs were anionic HCr<sub>2</sub>O<sub>7</sub><sup>–</sup>, HCrO<sub>4</sub><sup>–</sup>, CrO<sub>4</sub><sup>2–</sup>, and Cr<sub>2</sub>O<sub>7</sub><sup>2–</sup>, these ions could be attracted to the CPS surface due to electrostatic interaction [41]. In addition, it was reported that there might be some reduction of Cr(VI) to Cr(III) during adsorption due to –NH<sub>2</sub> groups, and then the Cr(III) could be immobilized because of coordination effects with –OH groups [42]. The representative diagram for mechanism is given in Fig. 8.

### 3.9. Comparison of CPS with other biomass adsorbents for Cr(VI) adsorption

Table 6 summarizes the comparison of adsorption capacities between CPS and other biomass adsorbents [43–54]. It was evident that the adsorption capacity of CPS was good and comparable with these adsorbents, which showed that peanut shell modified with citric acid was an effective adsorbent in the case of Cr(VI) removal.

### 3.10. Scale-up design

The scale-up design is established by using the mass balance equation, which can be calculated as [9,55]:

$$V(C_0 - C_i) = Wq_i \quad (19)$$

where  $V$  (L) is the volume of effluent;  $C_0$  (mg·L<sup>–1</sup>) is the initial Cr(VI) concentration;  $C_i$  (mg·L<sup>–1</sup>) is the Cr(VI) concentration

Table 4  
Parameters of different isotherms at 298 K

| Isotherm             | Parameters                   |                             |           |        |
|----------------------|------------------------------|-----------------------------|-----------|--------|
| Langmuir             | $q_m$ (mg·g <sup>–1</sup> )  | $b$ (L·mg <sup>–1</sup> )   | $R_L$     | $R^2$  |
|                      | 15.63                        | 1.1                         | 0.01–0.15 | 0.9961 |
| Freundlich           | $K_f$ (mg·g <sup>–1</sup> )  | $n$                         |           | $R^2$  |
|                      | 8.31                         | 1.32                        |           | 0.9958 |
| Dubinin–Radushkevich | $E$ (kJ·mol <sup>–1</sup> )  | $q_m$ (mg·g <sup>–1</sup> ) |           | $R^2$  |
|                      | 1.12                         | 7.67                        |           | 0.9769 |
| Temkin–Pyzhev        | $b_T$ (J·mol <sup>–1</sup> ) | $A$ (L·g <sup>–1</sup> )    |           | $R^2$  |
|                      | 994.8                        | 23.58                       |           | 0.9755 |

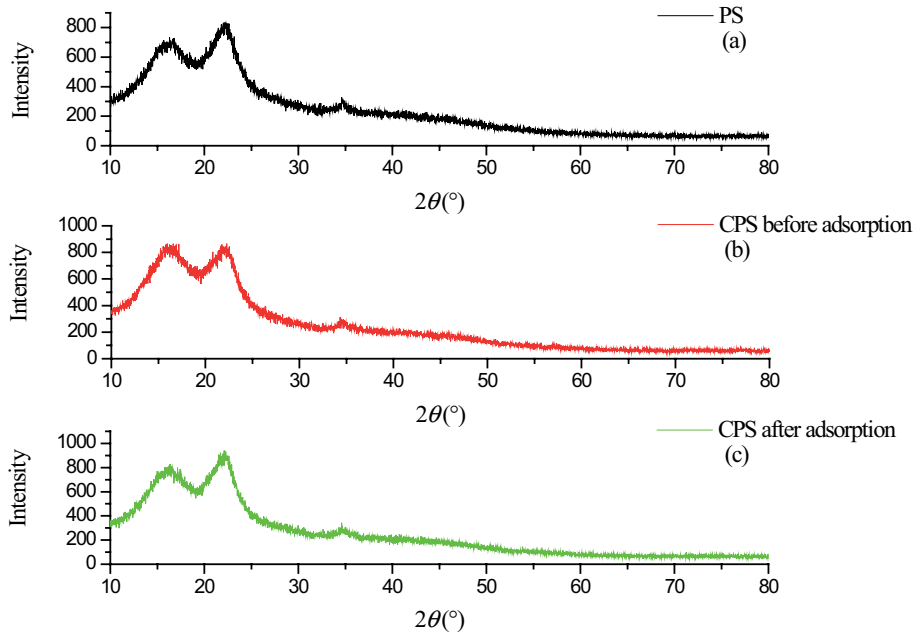


Fig. 6. XRD patterns: (a) PS, (b) CPS before adsorption, and (c) CPS after adsorption.

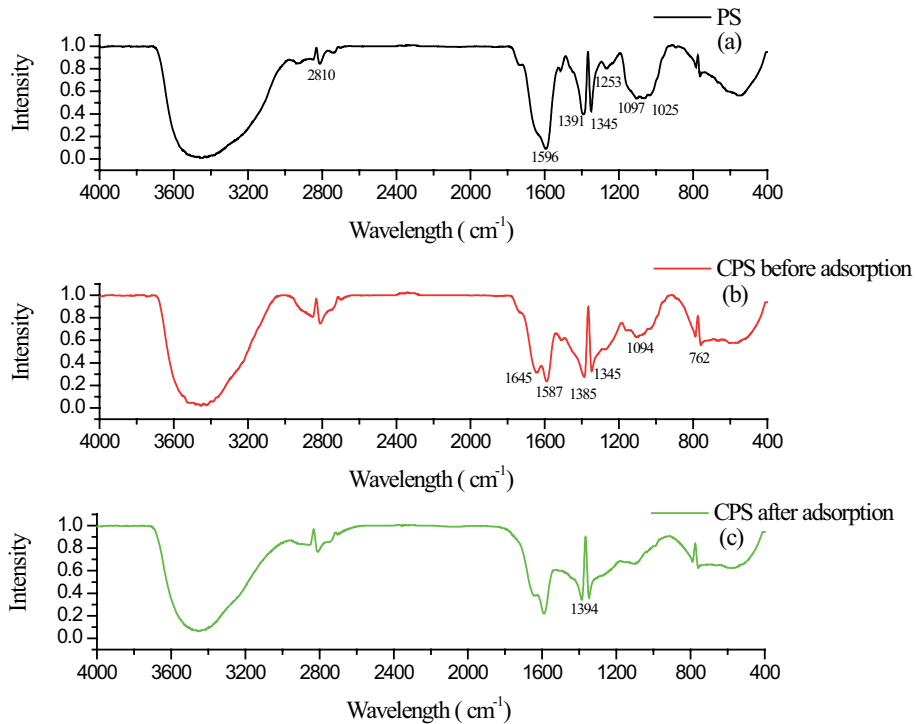


Fig. 7. FTIR spectra: (a) PS, (b) CPS before adsorption, and (c) CPS after adsorption.

Table 5  
Thermodynamic parameters for the Cr(VI) adsorption

| $\Delta H^\circ$        | $\Delta S^\circ$                        | $\Delta G^\circ$ (kJ·mol <sup>-1</sup> ) |         |         |         |         |
|-------------------------|---|--|---------|---------|---------|---------|
| (kJ·mol <sup>-1</sup> ) | (J·mol <sup>-1</sup> ·K <sup>-1</sup> ) | 298 (K)                                  | 308 (K) | 323 (K) | 338 (K) | 348 (K) |
| -11.31                  | -13.53                                  | -7.28                                    | -7.15   | -6.94   | -6.74   | -6.6    |

Table 6  
Comparison of adsorption capacities of CPS with other adsorbents for Cr(VI) adsorption

| No. | Adsorbents                                   | Cr(VI) adsorption capacity (mg·g <sup>-1</sup> ) | References    |
|-----|--|--|---------------|
| 1   | Banana peel                                  | 6.17   | [2]           |
| 2   | Oak acorn peel                               | 47.39  | [3]           |
| 3   | Chitosan-citric acid modified almond shell   | 100.3  | [15]          |
| 4   | Chitosan-citric acid modified hazelnut shell | 89.5   | [15]          |
| 5   | Sawdust                                      | 8.84   | [24]          |
| 6   | <i>Ulva compressa</i> L.                     | 21.66  | [32]          |
| 7   | Groundnut shell                              | 22.94  | [43]          |
| 8   | Walnut shell                                 | 24.52  | [43]          |
| 9   | Almond shell                                 | 24.25  | [43]          |
| 10  | Magnolia leaf                                | 3.96   | [44]          |
| 11  | Peanut shell                                 | 3.49   | [45]          |
| 12  | Hemicelluloses                               | 74.6   | [46]          |
| 13  | <i>Phanera vahlii</i> fruit biomass          | 159.1  | [47]          |
| 14  | Eucalyptus sawdust                           | 34.07  | [48]          |
| 15  | Corn straw                                   | 30.15  | [48]          |
| 16  | Corn cob                                     | 29.46  | [48]          |
| 17  | Pine cone                                    | 7.01–9.4   | [49]          |
| 18  | Corn husk                                    | 17.3   | [50]          |
| 19  | Mangosteen peel                              | 36.12  | [51]          |
| 20  | Corn cob                                     | 15.05  | [52]          |
| 21  | Green <i>Moringa</i> leaves                  | 33.9   | [53]          |
| 22  | Mango  | 69.52  | [54]          |
| 23  | Jackfruit                                    | 22.45  | [54]          |
| 24  | Rubber leaves                                | 15.79  | [54]          |
| 25  | Citric acid modified peanut shell            | 15.63  | Present study |

at time  $t$  (min);  $W$  (g) is the mass of adsorbent;  $q_t$  (mg·g<sup>-1</sup>) is the adsorption capacity.

As the process approaches equilibrium, the equation becomes:

$$V(C_0 - C_e) = Wq_e \quad (20)$$

where  $C_e$  (mg·L<sup>-1</sup>) is the Cr(VI) concentration at time  $t$  (min);  $q_e$  (mg·g<sup>-1</sup>) is the adsorption capacity at equilibrium.

The mass balance equation can be combined with the Langmuir isotherm equation to form the following equation:

$$\frac{W}{V} = \frac{(C_0 - C_e)(bC_e + 1)}{bC_e q_{\max}} \quad (21)$$

where  $b$  is the Langmuir constant;  $q_{\max}$  (mg·g<sup>-1</sup>) is the maximum adsorption capacity.

Table 7 shows the amount of CPS required for 99% removal of Cr(VI) at an initial concentration of 10 mg·L<sup>-1</sup>. Only 44.55 g of CPS might be used for 50 L of effluent.

### 3.11. Safe disposal of used adsorbents

The possible leaching of chromium ions from the used adsorbents may have an adverse effect on the environment, which needs to be investigated as well. In brief, the

Table 7  
Mass of CPS required for 99% Cr(VI) ions removal

| Initial Cr(VI) (mg·L <sup>-1</sup> ) | Volume of effluent (L) | Mass of CPS (g) |
|--------------------------------------|------------------------|-----------------|
| 10                                   | 10                     | 8.91            |
| 10                                   | 20                     | 17.82           |
| 10                                   | 30                     | 26.73           |
| 10                                   | 40                     | 35.64           |
| 10                                   | 50                     | 44.55           |

Cr(VI)-loaded CPS was incinerated for 1 h at approximately 600°C. After that, the obtained ash was mixed with deionized water in a liquid-solid ratio of 5:1 for 24 h [55–57]. And then the generated ash can be applied to road construction in the local city.

## 4. Conclusion

In this work, peanut shell powder was modified with citric acid and employed as an eco-friendly adsorbent (CPS) to remove Cr(VI) from aqueous solution. The adsorption capacity and efficiency of CPS for the removal of Cr(VI) were influenced by the dose of adsorbent, initial Cr(VI) concentration, and contact time. Furthermore, the study focused on adsorption equilibrium, kinetics,

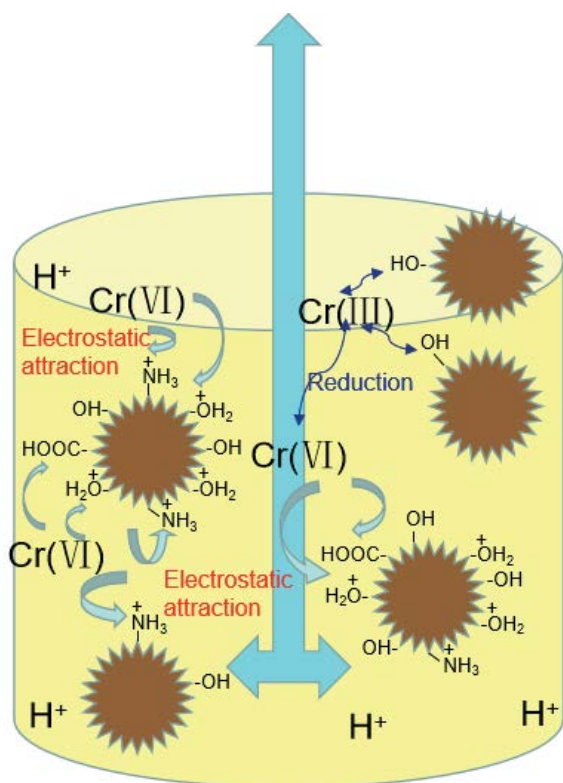


Fig. 8. Schematic diagram of adsorption mechanism.

and thermodynamics. The adsorption of Cr(VI) onto CPS was rapid in the first 90 min and then gradually reached equilibrium. Among the kinetic models that were put to the test, the pseudo-first-order, pseudo-second-order, and Elovich models provided good fits to the experimental data in the range of variables investigated. The results of the Weber–Morris and Boyd models suggested that intra-particle diffusion was not the only rate-determining step of Cr(VI) adsorption on CPS. Langmuir, Freundlich, Dubinin–Radushkevich, and Temkin isotherm models were applied to analyze the equilibrium data at 298 K. The results showed that the Langmuir model was more appropriate for Cr(VI) adsorption on CPS within the studied concentration range. The adsorptive capacity of CPS obtained by the Langmuir model was  $15.63 \text{ mg}\cdot\text{g}^{-1}$ . Thermodynamic parameters were calculated, revealing that the adsorption of Cr(VI) on CPS was a spontaneous and exothermic process. Based on the evidence of characterization, electrostatic attraction and reduction might be the main reasons for the adsorption. Additionally, only 44.55 g of CPS might be used for 50 L of effluent, indicating the cost-effective nature of this study. Hence, the overall outcome indicated that the citric acid modified peanut shell could be served as an efficient biosorbent to achieve the goal of waste control and Cr(VI) removal.

#### Declaration statement

#### Conflict of interest

The authors declare that they have no conflict of interest.

#### A data availability statement

The datasets generated during and/or analyzed during the current study are available from the corresponding author on reasonable request.

#### Authors' contributions

Qian Li (First Author) is responsible for Conceptualization, Methodology, Data curation, Writing Original draft. Qing Huang is responsible for Investigation, Data curation. Yifan Ruan is responsible for Writing-Reviewing and Editing.

#### Acknowledgement

The authors would like to thank the Hubei Key Laboratory of Purification and Application of Plant Anti-Cancer Active Ingredients for financial support.

#### References

- [1] S.J. Tshemese, W. Mhike, S.M. Tichapondwa, Adsorption of phenol and chromium(VI) from aqueous solution using exfoliated graphite: equilibrium, kinetics and thermodynamic studies, *Arabian J. Chem.*, 14 (2021) 103160, doi: 10.1016/j.arabj.2021.103160.
- [2] A. Ali, K. Saeed, F. Mabood, Removal of chromium(VI) from aqueous medium using chemically modified banana peels as efficient low-cost adsorbent, *Alexandria Eng. J.*, 55 (2016) 2933–2942.
- [3] S. Kuppusamy, P. Thavamani, M. Megharaj, K. Venkateswarlu, Y.B. Lee, R. Naidu, Oak (*Quercus robur*) acorn peel as a low-cost adsorbent for hexavalent chromium removal from aquatic ecosystems and industrial effluents, *Water Air Soil Pollut.*, 227 (2016) 62, doi: 10.1007/s11270-016-2760-z.
- [4] J. Kotaś, Z. Stasicka, Chromium occurrence in the environment and methods of its speciation, *Environ. Pollut.*, 107 (2000) 263–283.
- [5] J. Duan, H. Ji, T. Xu, F. Pan, X. Liu, W. Liu, D. Zhao, Simultaneous adsorption of uranium(VI) and 2-chlorophenol by activated carbon fiber supported/modified titanate nanotubes (TNTs/ACF): effectiveness and synergistic effects, *Chem. Eng. J.*, 406 (2021) 126752, doi: 10.1016/j.cej.2020.126752.
- [6] J.O. Ighalo, K.O. Iwuozor, C.A. Igwegbe, A.G. Adeniyi, Verification of pore size effect on aqueous-phase adsorption kinetics: a case study of methylene blue, *Colloids Surf., A*, 626 (2021) 127119, doi: 10.1016/j.colsurfa.2021.127119.
- [7] J. Cheng, Y. Leng, R. Gu, G. Yang, Y. Wang, X. Tuo, Adsorption of uranium(VI) from groundwater by amino-functionalized clay, *J. Radioanal. Nucl. Chem.*, 327 (2021) 1365–1373.
- [8] M. Banerjee, N. Bar, R.K. Basu, S.K. Das, Comparative study of adsorptive removal of Cr(VI) ion from aqueous solution in fixed bed column by peanut shell and almond shell using empirical models and ANN, *Environ. Sci. Pollut. Res.*, 24 (2017) 10604–10620.
- [9] A. Das, N. Bar, S.K. Das, Adsorptive removal of Pb(II) ion on *Arachis hypogaea's* shell: batch experiments, statistical, and GA modeling, *Int. J. Environ. Sci. Technol.*, (2022) 1–14, doi: 10.1007/s13762-021-03842-w.
- [10] S. Wang, H. Nam, H. Nam, Preparation of activated carbon from peanut shell with KOH activation and its application for H<sub>2</sub>S adsorption in confined space, *J. Environ. Chem. Eng.*, 8 (2020) 103683, doi: 10.1016/j.jece.2020.103683.
- [11] A. Das, N. Bar, S.K. Das, Pb(II) adsorption from aqueous solution by nutshells, green adsorbent: adsorption studies, regeneration studies, scale-up design, its effect on biological indicator and MLR modeling, *J. Colloid Interface Sci.*, 580 (2020) 245–255.
- [12] Ş. Parlayıcı, Modified peach stone shell powder for the removal of Cr(VI) from aqueous solution: synthesis, kinetic,

- thermodynamic, and modeling study, *Int. J. Phytorem.*, 21 (2019) 590–599.
- [13] M.T. Hoang, T.D. Pham, T.T. Pham, M.K. Nguyen, D.T. Nu, T.H. Nguyen, S. Bartling, B. Van der Bruggen, Esterification of sugarcane bagasse by citric acid for Pb<sup>2+</sup> adsorption: effect of different chemical pretreatment methods, *Environ. Sci. Pollut. Res.*, 28 (2020) 11869–11881.
- [14] A. Tehrim, M. Dai, X. Wu, M.M. Umair, I. Ali, M.A. Amjed, R. Rong, S.F. Javaid, C. Peng, Citric acid modified waste cigarette filters for adsorptive removal of methylene blue dye from aqueous solution, *J. Appl. Polym. Sci.*, 138 (2021) 50655, doi: 10.1002/app.50655.
- [15] T. Altun, H. Ecevit, B. Çiftçi, Production of chitosan coated, citric acid modified almond, and hazelnut shell adsorbents for Cr(VI) removal and investigation of equilibrium, kinetics, and thermodynamics of adsorption, *Arabian J. Geosci.*, 14 (2021) 439, doi: 10.1007/s12517-021-06631-4.
- [16] T. Qi, L. Pan, T. Sheng, L. Chuan-qiang, Study of citric acid modified peanut shell as Cr(VI) adsorbent, *Appl. Chem. Ind. (Xi'an, China)*, 49 (2020) 1088–1091.
- [17] S. Wang, L. Wang, W. Kong, J. Ren, C. Liu, K. Wang, R. Sun, D. She, Preparation, characterization of carboxylated bamboo fibers and their adsorption for lead(II) ions in aqueous solution, *Cellulose*, 20 (2013) 2091–2100.
- [18] Y. He, P. Wu, W. Xiao, G. Li, J. Yi, Y. He, C. Chen, P. Ding, Y. Duan, Efficient removal of Pb(II) from aqueous solution by a novel ion imprinted magnetic biosorbent: adsorption kinetics and mechanisms, *PLoS One*, 14 (2019) e0213377, doi: 10.1371/journal.pone.0213377.
- [19] U.A. Edet, A.O. Ifelebuegu, Kinetics, isotherms, and thermodynamic modeling of the adsorption of phosphates from model wastewater using recycled brick waste, *Processes*, 8 (2020) 665, doi: 10.3390/pr8060665.
- [20] M. Manjuladevi, R. Anitha, S. Manonmani, Kinetic study on adsorption of Cr(VI), Ni(II), Cd(II) and Pb(II) ions from aqueous solutions using activated carbon prepared from *Cucumis melo* peel, *Appl. Water Sci.*, 8 (2018) 36, doi: 10.1007/s13201-018-0674-1.
- [21] I. Zinicovscaia, N. Yushin, D. Grozdov, K. Boldyrev, E. Rodlovskaya, T.M. Ostrovnyaya, Removal of metals from synthetic and real galvanic nickel-containing effluents by *saccharomyces cerevisiae*, *Chem. Ecol.*, 37 (2020) 83–103.
- [22] H. Shi, L. Weisong, L. Zhong, C.J. Xu, Methylene blue adsorption from aqueous solution by magnetic cellulose/graphene oxide composite: equilibrium, kinetics, and thermodynamics, *Ind. Eng. Chem. Res.*, 53 (2014) 1108–1118.
- [23] A.A. Alghamdi, A.-B. Al-Odayni, W.S. Saeed, A. Al-Kahtani, F.A. Alharthi, T. Aouak, Efficient adsorption of lead(II) from aqueous phase solutions using polypyrrole-based activated carbon, *Materials*, 12 (2019) 2020, doi: 10.3390/ma12122020.
- [24] R. Chakraborty, R. Verma, A. Asthana, S.S. Vidya, A.K. Singh, Adsorption of hazardous chromium(VI) ions from aqueous solutions using modified sawdust: kinetics, isotherm and thermodynamic modeling, *Int. J. Environ. Anal. Chem.*, 101 (2019) 911–928.
- [25] W. Wang, Equilibrium, kinetics and thermodynamics study on the adsorption of Cr(VI) and As(III) by diatomite-modified MnO<sub>2</sub>, *J. Dispersion Sci. Technol.*, 43 (2020) 859–872.
- [26] X. Liu, L. Xu, Y. Liu, W. Zhou, Synthesis of citric acid-modified resins and their adsorption properties towards metal ions, *R. Soc. Open Sci.*, 5 (2018) 171667, doi: 10.1098/rsos.171667.
- [27] S. Ibrahim, M.A. Hanafiah, F. Fadzil, Adsorption of lead ions onto citric acid modified rubber (*Hevea brasiliensis*) leaves, *Adv. Mater. Res.*, 896 (2014) 288–291.
- [28] W.Q. Tang, R.Y. Zeng, Y.L. Feng, W. Wu, X.X. Wang, X. Li, Adsorption of Cu<sup>2+</sup> from aqueous solution by polyacid modified shaddock skin, *Chin. J. Process Eng.*, 12 (2012) 776–780.
- [29] A. Günay, E. Arslankaya, İ. Tosun, Lead removal from aqueous solution by natural and pretreated clinoptilolite: adsorption equilibrium and kinetics, *J. Hazard. Mater.*, 146 (2007) 362–371.
- [30] H. Deng, L. Yang, G. Tao, J. Dai, Preparation and characterization of activated carbon from cotton stalk by microwave assisted chemical activation-application in methylene blue adsorption from aqueous solution, *J. Hazard. Mater.*, 166 (2009) 1514–1521.
- [31] A.D. Aderibigbe, O. Ogunlalu, O.O. Oluwasina, I.A. Amoo, Adsorption studies of Pb<sup>2+</sup> from aqueous solutions using unmodified and citric acid – modified plantain (*Musa paradisiaca*) peels, *IOSR J. Appl. Chem.*, 10 (2017) 30–39.
- [32] A. Aid, S. Amokrane, D. Nibou, E. Mekatel, M. Trari, V. Hulea, Modeling biosorption of Cr(VI) onto *Ulva compressa* L. from aqueous solutions, *Water Sci. Technol.*, 77 (2018) 60–69.
- [33] K.L. Wasewar, M. Atif, B. Prasad, I.M. Mishra, Adsorption of zinc using tea factory waste: kinetics, equilibrium and thermodynamics, *Clean – Soil, Air, Water*, 36 (2008) 320–329.
- [34] P. Wang, Q. Ma, D. Hu, L. Wang, Adsorption of methylene blue by a low-cost biosorbent: citric acid modified peanut shell, *Desal. Water Treat.*, 57 (2016) 10261–10269.
- [35] M.M. Golor, D. Rosma, S.P. Santoso, F. Soetaredjo, M. Yuliana, S. Ismadji, A. Ayucitra, Citric acid-crosslinked cellulosic hydrogel from sugarcane bagasse: preparation, characterization, and adsorption study, *J. Indonesian Chem. Soc.*, 3 (2020) 59–67.
- [36] L. Guo, L. Liang, Y. Wang, M. Liu, Biosorption of Pb<sup>2+</sup> from aqueous solution by rice straw modified with citric acid, *Environ. Prog. Sustainable Energy*, 35 (2016) 359–367.
- [37] P. Utomo, N.M. Nizado, E. Saepudin, Crosslink modification of tapioca starch with citric acid as a functional food, *AIP Conf. Proc.*, 2242 (2020) 040055, doi: 10.1063/5.0010364.
- [38] K. Ghosh, N. Bar, A.B. Biswas, S.K. Das, Elimination of crystal violet from synthetic medium by adsorption using unmodified and acid-modified eucalyptus leaves with MPR and GA application, *Sustainable Chem. Pharm.*, 19 (2021) 100370, doi: 10.1016/j.scp.2020.100370.
- [39] L. Leng, S. Xu, R. Liu, T. Yu, X. Zhuo, S. Leng, Q. Xiong, H. Huang, Nitrogen containing functional groups of biochar: an overview, *Bioresour. Technol.*, 298 (2020) 122286, doi: 10.1016/j.biortech.2019.122286.
- [40] W. Wang, J. Hu, R. Zhang, C. Yan, L. Cui, J. Zhu, A pH-responsive carboxymethyl cellulose/chitosan hydrogel for adsorption and desorption of anionic and cationic dyes, *Cellulose*, 28 (2021) 897–909.
- [41] B. Singha, N. Bar, S.K. Das, The use of artificial neural networks (ANN) for modeling of adsorption of Cr(VI) ions, *Desal. Water Treat.*, 52 (2014) 415–425.
- [42] C. Lin, W. Luo, T. Luo, Q. Zhou, H. Li, L. Jing, A study on adsorption of Cr(VI) by modified rice straw: characteristics, performances and mechanism, *J. Cleaner Prod.*, 196 (2018) 626–634.
- [43] A. Das, M. Banerjee, N. Bar, S.K. Das, Adsorptive removal of Cr(VI) from aqueous solution: kinetic, isotherm, thermodynamics, toxicity, scale-up design, and GA modeling, *SN Appl. Sci.*, 1 (2019) 776, doi: 10.1007/s42452-019-0813-9.
- [44] N.K. Mondal, A. Samanta, P. Roy, B. Das, Optimization study of adsorption parameters for removal of Cr(VI) using *Magnolia* leaf biomass by response surface methodology, *Sustainable Water Resour. Manage.*, 5 (2019) 1627–1639.
- [45] B. Rzig, F. Guesmi, M. Sillanpää, B. Hamrouni, Modelling and optimization of hexavalent chromium removal from aqueous solution by adsorption on low-cost agricultural waste biomass using response surface methodological approach, *Water Sci. Technol.*, 84 (2021) 552–575.
- [46] Y. Wei, W. Chen, C. Liu, H. Wang, Facial synthesis of adsorbent from hemicelluloses for Cr(VI) adsorption, *Molecules*, 26 (2021) 1443, doi: 10.3390/molecules26051443.
- [47] A. Ajmani, T. Shahnaz, S. Subbiah, S. Narayanasamy, Hexavalent chromium adsorption on virgin, biochar, and chemically modified carbons prepared from *Phanera vahlii* fruit biomass: equilibrium, kinetics, and thermodynamics approach, *Environ. Sci. Pollut. Res.*, 26 (2019) 32137–32150.
- [48] S. Khushk, L. Zhang, A.M. Pirzada, M. Irfan, A. Li, Cr(VI) heavy metal adsorption from aqueous solution by KOH treated hydrochar derived from agricultural wastes, *AIP Conf. Proc.*, 2119 (2019) 020003, doi: 10.1063/1.5115362.
- [49] A. Pholosi, E.B. Naidoo, A.E. Ofomaja, Kinetics and Mechanism of Cr(VI) Adsorption onto NaOH Treated Pine and Magnetite-Pine Composite, P. Ramasami, M. Gupta Bhowon, S. Jhaumeer

- Laulloo, H. Li Kam Wah, Eds., International Conference on Pure and Applied Chemistry, ICPAC 2018: Chemistry for a Clean and Healthy Planet, Springer, Cham, 2019, pp. 469–488.
- [50] J.N. Zarur, C.T. Tovar, Á.V. Ortiz, D. Acevedo, R.E. Tejada Tovar, Thermodynamics, kinetics and equilibrium adsorption of Cr(VI) and HG(II) in aqueous solution on corn husk (*Zea mays*), *Int. J. ChemTech Res.*, 11 (2018) 265–280.
- [51] U. Haura, F. Razi, H. Meilina, Adsorbent characterization from mangosteen peel and its adsorption performance on Pb(II) and Cr(VI), *Biopropal Ind.*, 8 (2017) 47–54.
- [52] Á. Villabona-Ortiz, C. Tejada Tovar, A. Herrera-Barros, Á.D. González-Delgado, J. Nunez-Zarur, Kinetic and dynamic study of Cr(VI) adsorption onto chemically modified corn cob, *Contemp. Eng. Sci.*, 11 (2018) 1383–1391.
- [53] C.C. Timbó, M. Kandawa-Schulz, M. Amuanyena, H.M. Kwaambwa, Adsorptive removal from aqueous solution of Cr(VI) by Green *Moringa* tea leaves biomass, *J. Encapsulation Adsorpt. Sci.*, 7 (2017) 108–119.
- [54] S. Nag, N. Bar, S.K. Das, Cr(VI) removal from aqueous solution using green adsorbents in continuous bed column – statistical and GA-ANN hybrid modeling, *Chem. Eng. Sci.*, 226 (2020) 115904, doi: 10.1016/j.ces.2020.115904.
- [55] M. Banerjee, N. Bar, R.K. Basu, S.K. Das, Removal of Cr(VI) from its aqueous solution using green adsorbent pistachio shell: a fixed bed column study and GA-ANN modeling, *Water Conserv. Sci. Eng.*, 3 (2017) 19–31.
- [56] T. Mitra, N. Bar, S.K. Das, Rice husk: green adsorbent for Pb(II) and Cr(VI) removal from aqueous solution—column study and GA-NN modeling, *SN Appl. Sci.*, 1 (2019) 486, doi: 10.1007/s42452-019-0513-5.
- [57] S. Sarkar, N. Bar, S.K. Das, Cr(VI) and Cu(II) removal from aqueous solution in fixed bed column using rice bran; experimental, statistical and GA modeling, *J. Indian Chem. Soc.*, 98 (2021) 100216, doi: 10.1016/j.jics.2021.100216.